Dalton Transactions

ROYAL SOCIETY OF CHEMISTRY

PAPER

View Article Online
View Journal

Cite this: DOI: 10.1039/d6dt01038e

A non-innocent radical-anionic nitrosoarene ligand regularizes a formal palladium(I) complex to palladium(II)

Doaa R. Ramadan, [a,b] Manar Ahmed Fouad, [a,b] Francesco Ferretti, [a] Artur Brotons Rufes, [c] Piero Macchi, [d] Lorenzo Sorace, [e] Martí Gimferrer, [f] Chiara Costabile *[c] and Fabio Ragaini *[a]

Received 4th May 2026,
Accepted 22nd May 2026

DOI: 10.1039/d6dt01038e

rsc.li/dalton

Attempts to synthesize a phenanthroline palladium(0) complex with an η^2-coordinated nitrosoarene starting from a palladium(II) precursor and the corresponding aryl hydroxylamine afforded instead apparent palladium(I) metallacyclic complexes that, on a closer inspection, were proven to be Pd(II) complexes with a new kind of radical-anionic nitrosoarene ligand.

Introduction

Monomeric palladium complexes with η^2-ArNO ligands have been proposed to be intermediates in many reactions in which the corresponding nitroarene is reduced and in some cases carbonylated to yield N-heterocycles, isocyanates, carbamates, or ureas.[1–3] However, only a few of them have been isolated and fully characterized and they all show the same general formula $Pd(CNAr^{Dipp2})_2(\eta^2\text{-ArNO})$ (Dipp = 2,6-(i-Pr)$_2$C$_6$H$_3$)[4,5] in which the very hindered isonitrile ligand is not suitable for the reported catalytic reactions. In the past years we made several attempts to generate Pd(Phen)(PhNO) (Phen = 1,10-phenanthroline), but we always obtained a polymeric material of apparent composition $Pd_2(Phen)_2(PhNO)_3$.[6] Since this product may derive from a reaction of the initially formed Pd(Phen)(PhNO) with excess nitrosobenzene, we more recently attempted to generate the desired complex by the reaction of a palladium(II) precursor, $Pd(Phen)(NO_3)_2$, with phenyl hydroxylamine. However, the nitrate ligand became involved in the oxidation of the hydroxylamine and a metallacycle with a κ^2O, O-ONN(Ar)O ligand was formed, where the obtained nitrosoarene was coupled to a NO_3^- derived NO.[7] In order to avoid this problem, we investigated the reaction of aryl hydroxylamines with $Pd(Phen)(OAc)_2$.

Results and discussion

The employed hydroxylamines were synthesized following an adapted procedure reported in the literature.[8] The reaction was carried out in a water–ethanol mixture at room temperature using sodium borohydride as the reducing agent to convert nitroarenes into various nitrogen-containing compounds. Highly active palladium nanoclusters (Pd NCs), generated *in situ* by the reduction of $Pd(OAc)_2$ by $NaBH_4$, were employed as the catalyst. By carefully controlling the water-to-ethanol ratio (H_2O : ethanol = 3 : 2), hydroxylamines could be selectively obtained with yields of up to 90%.

When $Pd(Phen)(OAc)_2$, dissolved in MeCN, was treated with an equimolar amount of *p*-cyanophenyl hydroxylamine at r.t., the solution gradually turned from yellow to dark green. After one hour, stirring was interrupted and diethyl ether was layered on the MeCN solution, resulting in the formation of single crystals of a new compound (**2a**) and of unreacted $Pd(Phen)(OAc)_2$. Repeating the reaction in the presence of Et_3N did not change its outcome, but the reaction could be pushed to completion by employing a threefold excess of hydroxylamine.

Single crystal X-ray diffraction showed that **2a** is a mononuclear neutral complex containing a phenyl-*o*-nitrosophenylamide ligand. The latter results from the N–C coupling of two arylhydroxylamine moieties, one of which is coordinated as an amido group and the other as an η^1-ArNO moiety (Scheme 1a and Fig. 1). η^1-Nitrosoarenes are generally considered to coordinate as neutral ligands.[9] Assuming that the amido group acts as an anionic ligand, this would imply that **2a** is a very rare case of a monomeric palladium(I) complex.[10] The coordi-

[a]Dipartimento di Chimica, Università di Milano, V. C. Golgi 19, 20133 Milano, Italy. E-mail: fabio.ragaini@unimi.it
[b]Chemistry Department, Faculty of Science, Alexandria University, P.O. Box 426, Alexandria 21321, Egypt
[c]Dipartimento di Chimica e Biologia "A. Zambelli", Università di Salerno, V. Giovanni Paolo II, 84084 Fisciano, SA, Italy. E-mail: ccostabile@unisa.it
[d]Dipartimento di Chimica, Materiali e Ingegneria Chimica, Politecnico di Milano, V. Bassini 6b, 20133 Milano, Italy
[e]Dipartimento di Chimica "Ugo Schiff" & Udr INSTM Università di Firenze Via della Lastruccia 3-13, 50019 Sesto Fiorentino, FI, Italy
[f]Institut für Physikalische Chemie, Georg-August Universität, Göttingen, Tammanstr. 6, Göttingen 37077, Germany

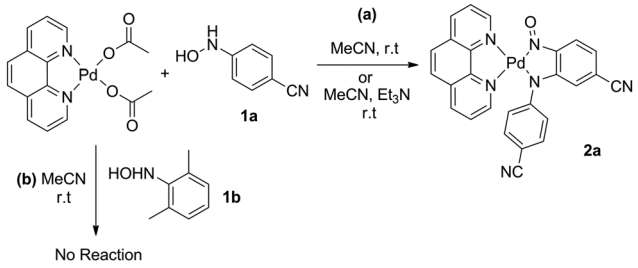

Scheme 1 Reactions of Pd(Phen)$(OAc)_2$ with aryl hydroxylamines.

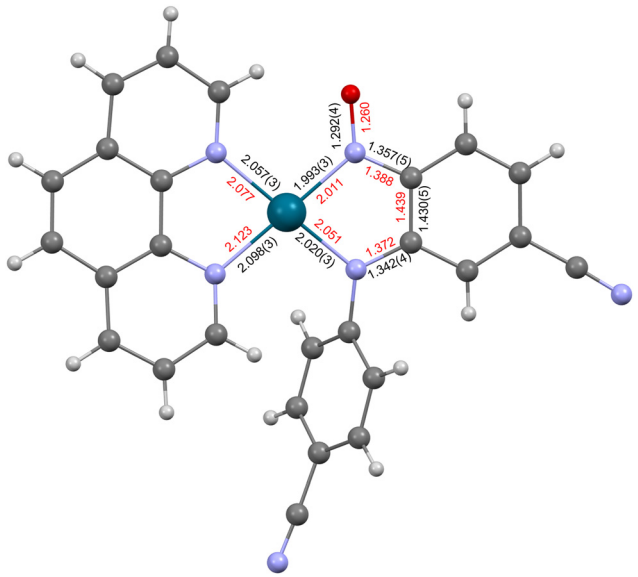

Fig. 1 The geometry of **2a** determined from single crystal X-ray diffraction. The most relevant bond distances (in Å) are reported (with estimated standard deviations in parentheses). Calculated distances are reported in red.

nation geometry around the metal ion is distorted square planar, which is typical of Pd(II) complexes, but is also compatible with a tetracoordinate Pd(I) complex.[11,12] Since the complex is neutral, an odd electron count results and it has to be paramagnetic, either because palladium is in a +1 oxidation state or because of the formation of a radical-anionic nitroso ligand in conjunction with a +2 oxidation state of the palladium.

Interestingly, only three complexes, related to each other, have been reported in the literature containing a ligand analogous to that present in **2a**.[13,14] A structural characterization is available for only one of them, featuring no substituent on the aryl rings. It is a dimeric Pd complex, $[(\kappa^2N,N\text{-}2\text{-}PhN\text{-}C_6H_4NO)Pd]_2(\mu_2\text{-}OAc)_2$,[14] with two bridging acetate ligands, for which the standard +2 oxidation state could be inferred, in agreement with its diamagnetic nature.

The N–O distance in the dimeric palladium complex mentioned above is 1.24(1) Å, comparable with the corresponding distance in the independently synthesized free ligand, 1.259(2) Å,[15] confirming its double bond character. The N–O bond length in **2a** is somewhat longer, 1.292(4) Å, still quite shorter than that in the only structurally characterized palladium η^2-ArNO complexes, 1.334–1.354 Å depending on the substituents on the aryl ring, and for which a Pd(II) with a di-anionic nitrosoarene ligand electronic configuration has been proposed.[4,5] However, it is almost coincident with that reported for *trans*-Pd$(CNAr^{Dipp2})_2(\eta^1\text{-}PhNO)_2$, 1.291(2) Å,[16] for which a Pd(II) configuration has been proven, with two radical-anionic nitrosobenzene ligands and in which a N–O bond order of 1.5 could be assigned.[4,16] The radical chemistry of nitrosoarenes, either metal-mediated or not, has important synthetic implications,[17] but only a handful of complexes with a radical-anionic ArNO ligand have been structurally characterized.[4,5,18–20]

To ascertain the true nature of **2a**, a Pd(I) complex or a Pd(II) complex with a radical-anionic nitroso ligand, and to gain more insight into the electronic distribution, spectroscopic characterization and theoretical calculations were carried out.

The Continuous Wave Electron Paramagnetic Resonance (cw-EPR) spectra at the X-band ($\nu \approx 9.4$ GHz) collected both on solution and polycrystalline powder samples of **2a** at cryogenic and room temperature unequivocally indicate that the spin density of **2a** is located on the organic moiety. Indeed, the solid state spectrum (Fig. S5) is nicely reproduced[21] by assuming a spin $S = 1/2$ with $g_{xy} = 2.000(1)$ and $g_z = 2.019(2)$, which is consistent with values expected for a nitroso radical.[22] Interestingly, while the solid-state spectrum shows clear evidence of a half field transition (inset of Fig. S5), this is absent in the frozen solution spectrum (Fig. 2, upper panel), indicating that intermolecular interactions are active in the solid state but not in the solvent. Inspection of the crystal packing suggests that these may arise following π-stacking interactions between pairs of neighbouring molecules lying on parallel planes.

The frozen solution spectrum could be nicely reproduced[21] by assuming completely rhombic **g** and a hyperfine coupling tensor to ^{14}N ($I = 1$) (Fig. 2, upper panel). Finally, the simulation of the second derivative of the fluid solution spectrum (Fig. 2, lower panel) provided the isotropic hyperfine coupling parameters to the nitroso ^{14}N ($I = 1$), a single ^1H ($I = 1/2$) which we attribute to the *ortho* proton (*vide infra*) and to ^{105}Pd ($I = 5/2$, n. ab. = 22%). The obtained values (see Table 1) for isotropic and anisotropic hyperfine coupling, which are consistent with expectations for a nitrosoarene anion radical,[5,23,24] allowed us to calculate a spin density on ^{14}N of about 33% (see the SI for details of the calculations), whereas the very small value of the coupling to ^{105}Pd confirms the coordination of the radical in solution and indicates a very small spin density on the metal ion.

Using the X-ray structure of **2a** as a starting guess, DFT calculations were performed to optimize the geometry at the uM06-D3/def2-TZVPP//uBP86/def2-SVP level of theory (see the SI for computational details and method validation).

The DFT calculations of the EPR parameters were run with ORCA, according to the computational details reported in the SI. The computed *g*-tensor exhibits only moderate anisotropy, with principal values $g_x = 1.988$, $g_y = 1.996$, and $g_z = 2.015$ ($g_{iso} = 2.000$) remaining close to the free-electron values. Although computed *g*

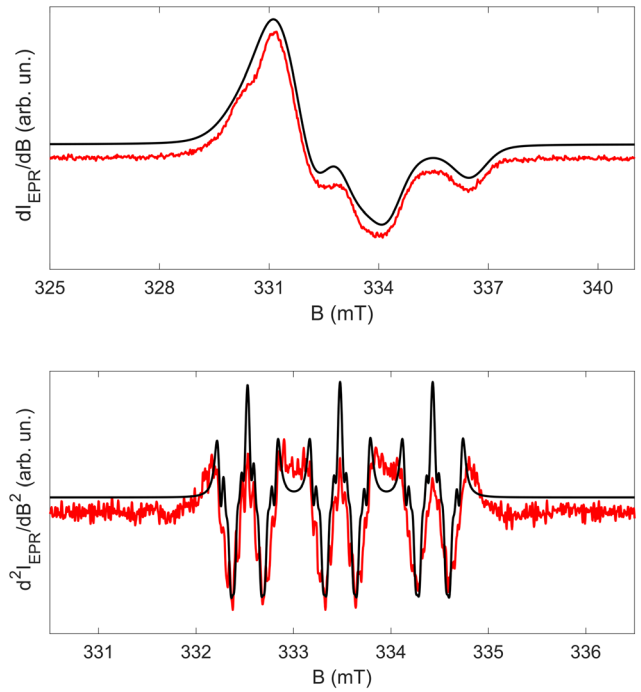

Fig. 2 Experimental (red lines) X-band EPR spectra of **2a** dissolved in CH_2Cl_2 : toluene, 1 : 1 (*ca.* 1 mM), and best simulations obtained using parameters reported in Table 1 (black line). Upper panel: spectrum measured at 20 K. ν = 9.356 GHz, power = 2.696 μW, and modulation amplitude: 0.15 mT. Lower panel: spectrum measured at room temperature and reported as a second derivative of the absorption ν = 9.376 GHz, power: 6.779 mW, and modulation amplitude: 0.01 mT.

Table 1 Best simulation spin Hamiltonian parameters for the EPR spectra of **2a** under different conditions, and DFT calculated parameters (detailed DFT values in Table S12)

	Powder	Frozen solution	Fluid solution	DFT
g_x	2.002	2.000		1.988
g_y	2.002	2.007		1.996
g_z	2.019	2.019		2.015
g_{iso}	—	—	2.0088	2.000
$\lvert A_x(^{14}N)\rvert$/MHz	—	62.2		63.2
$\lvert A_y(^{14}N)\rvert$/MHz	—	6.80		9.4
$\lvert A_z(^{14}N)\rvert$/MHz	—	11.5		7.3
$\lvert A_{iso}(^{14}N)\rvert$/MHz	—	—	26.7	26.6
$\lvert A_{iso}(^{1}H)\rvert$/MHz		—	8.75	13.9
$\lvert A_{iso}(^{105}Pd)\rvert$/MHz		—	1.3	3.7

values are slightly underestimated with respect to the experimental ones, the deviation remains within the typical accuracy of DFT for *g* tensors and reproduces the overall anisotropy and ordering of the tensor components. The DFT calculated parameters for the hyperfine coupling to Pd, N (of the nitroso group, namely N6 of Fig. 4) and H *ortho* to the nitroso group (namely H15 of Fig. 4) are in good agreement with experimental ones.

Molecular orbital (MO) analysis reveals that the unpaired electron corresponding to the highest occupied MO (HOMO) is mostly located on the nitroso-containing metallacycle ligand, with a very small contribution from the metal centre (Fig. S8). Moreover, the three lower energy molecular orbitals result from the overlap between the d-type Pd orbitals and the σ- and π-system of the phenyl-*o*-nitrosophenylamide ligand (Table S3). The spin density distribution (see Fig. 3) indicates that most of the excess spin is located on the nitroso ligand and especially on the N–O group itself with only minor spin density around the metal. This suggests a nitroso-centered radical, consistent with a formal Pd(II) center, although a strict assignment of these orbitals to either the metal or ligand is complicated by their delocalized character.

A plausible solution is the use of computational tools specifically devised to assign formal oxidation states or quantify the local spin of each atom/fragment in the molecule, such as the Effective Oxidation State (EOS) and Local Spin Analysis (LSA), which proved their usefulness in the characterization of challenging organometallic compounds.[25–27] These methods, implemented in the APOST-3D software,[28] require defining the atom in a molecule (AIM) and manually selecting which atoms constitute a given fragment. In this work, we used the Topological Fuzzy Voronoi Cells (TFVC) AIM definition[29,30] and selected the three chemically intuitive fragments shown in Fig. 4. The TFVC charges of each fragment are shown in Table S4. The palladium centre presents an atomic charge very close to +1 (1.107), being the negative counterpart mostly located in fragment **3** (−1.208), whereas fragment **2** was found to be almost perfectly neutral (0.097). This describes a coordinated complex with a cationic metal centre and an anionic ligand, as expected. Moreover, N6 has a charge of −0.473, which fits with a σ-donation to an electron-deficient metal centre that struggles to back-donate, as a Pd(II) (Table S5). The vicinal N4 has a considerably greater negative charge of ∼−1.3,

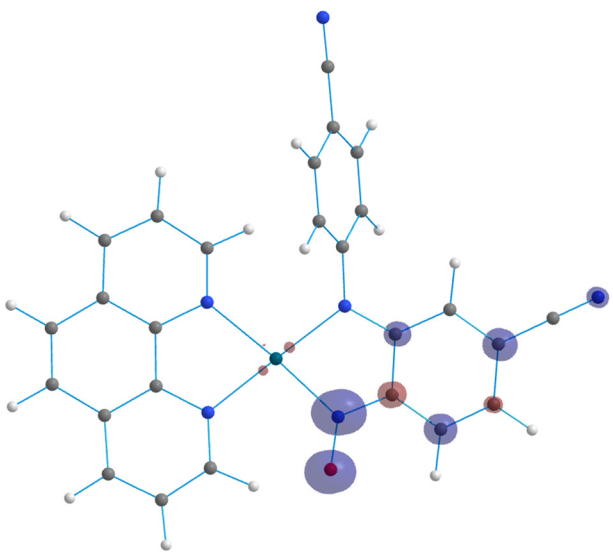

Fig. 3 The 3D spin density distribution ($\rho^{\sigma}(r) = \rho_{\alpha}(r) - \rho_{\beta}(r)$). The isosurface value is ±0.01 e Bohr^{-3} (transparent blue is positive and transparent red is negative). Note that most of the spin density is resident on fragment **3** and especially on the N–O group. Only a very small contribution is visible in the vicinity of the Pd atom.

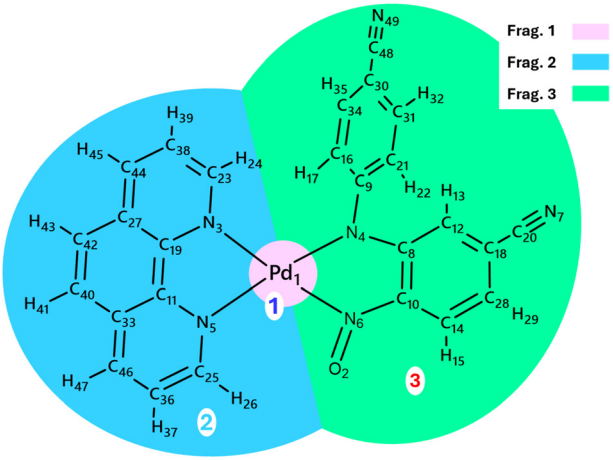

Fig. 4 Fragment definition for chemical bonding calculations.

which is expected for an amide nitrogen. A similar situation occurs in fragment **2**, where the two nitrogen atoms have even more negative charges of ∼−1.4. These large negative values do not indicate an actual anionic character; rather, a consequence of a real-space partition of an electronegative atom in a highly delocalized system as a phenanthroline. Conversely, for the nitroso nitrogen, the charge decreases due to the delocalization within the N6 and O2 bond. So far, it has been possible to describe the overall electron density distribution among fragments, but no indication of unpaired electron density distribution can be found yet.

To clarify or ensure the formal electronic picture of the system, we used a tool especially designed for that purpose: the effective oxidation state (EOS). This method treats the electrons in the same orbital with opposite spin (α and β) independently, making it possible to assign them separately to each atom of a molecule. The EOS analysis is based on effective fragment orbitals (EFOs) and their occupation numbers, calculated for all fragments defined in the system. This is another methodology designed to account for oxidation states by treating the electrons individually. These are assigned to those spin-resolved EFOs, which have been previously ordered by their occupations. This procedure yields an effective electronic configuration for each atom or ligand in the molecule, which directly determines its oxidation state. A reliability index (*R*%) is used to assess how close the *real* electronic structure of the complex is to the *formal* one (based on the ionic assignment of electrons), calculating the difference between the occupation number of the last occupied (LO) and the first unoccupied (FU) EFOs. When this gap is very small, the localization of the electron in a single orbital is dubious. The most problematic scenario arises when two or more frontier EFOs located on different fragments share the same occupation number. In such cases, EOS analysis produces two equally plausible oxidation state distributions, with $R = 50\%$.

The first relevant possible observation concerns the number of α and β occupied EFOs reported in the output, where fragment **3** shows an odd number of orbitals, which contrasts with the even number of elements for fragments **1** and **2** (see Tables S6 and S7). This already suggests that the unpaired electron does not belong to fragment **1** (*i.e.* Pd). When looking at its valence d-orbitals, we see four α and β pairs with high occupations (Fig. S10). Then, with a much lower value, one finds the empty $4d_{|x^2-y^2|}$, which is typical of a Pd(II) electronic configuration and a square planar coordination. The 5s orbital displays an even lower occupation (0.128–0.129).

In all three fragments, there are several orbitals with very low occupations, low enough not to compete in the electronic assignation (formally virtual orbitals, with occupations presented in Tables S6–S8). Overall, the *R*(%) value is 68.95, which is somewhat low but larger than the threshold for the electron being considered clear-cut (>60%).[31]

It is important to note that the occupation ordering of the EFOs is not in a 1 : 1 correspondence with the canonical orbitals, which are variationally ordered with respect to the energy. So, the last occupied EFO (LO), presented in Fig. 5 left, does not correspond to the unpaired electron, having also a complementary β EFO with a matching isosurface (occupation in parentheses). To find the unpaired electron, we have to search for an orbital without a complement within the occupied EFOs. This is a consequence of the EFOs being ordered by decreasing occupation. The α EFO of significant occupation that lacks an occupied complement is displayed in Fig. 5 right. Note how the shape of the orbital is similar to the last occupied canonical MO shown in Fig. S9, but much more localized in the nitroso group and binding nitrogen.

Overall, the EOS analysis assigns a formal oxidation state of −2 to the nitrosamido ligand (fragment **3**), and +2 to the palladium centre (fragment **1**), with the unpaired electron (radical) being located on the nitroso ligand. This is in agreement with the experimental EPR findings.

Further characterization of the unpaired electron in **2a** can be realized by means of the local spin analysis and the number of the effectively unpaired electrons.[32] The results are presented in Table S9, pinpointing that the unpaired electron is mostly on fragment **3** (91.4%), with only a 4% located at the Pd centre. These values harshly contradict a Pd(I) situation and are consistent with EPR results. Evaluating the contri-

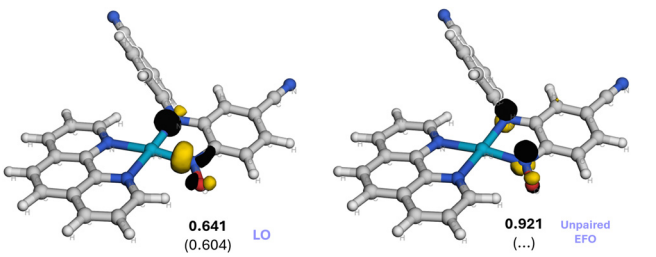

Fig. 5 Relevant effective fragment orbitals (EFOs) of the nitrosamido ligand (fragment **3**): last occupied EFO (left) and unpaired EFO (right). The latter corresponds to the unpaired electron of the system.

bution per atom, one can see that more than half of the unpaired density comes from the nitroso functional group with 29.4% on N and 27.9% on O, respectively (Table S10). Note that the calculated 29.4% unpaired density on nitrogen is in excellent agreement with the *ca.* 33% value obtained by the simulation of the fluid solution EPR spectrum (*vide supra*). Furthermore, the impact of the cyanide substituents was evaluated on the unsubstituted analogue. Although some of the unpaired density moves towards the phenanthroline side, most of it remains unchanged.

Finally, the $\langle S^2 \rangle$ value of the wavefunction at the current level of theory is 0.781 (0.75 ideal value for a doublet). Its decomposition by means of local spin analysis, with $\langle S^2 \rangle_A$ being the *A*-th fragment contribution to the total $\langle S^2 \rangle$, allows unveiling the location of the unpaired electron. In particular, an ideal fragment with one unpaired electron (doublet) leads to $\langle S^2 \rangle_A$ = 0.75, while a fragment with all electrons paired (singlet) shows $\langle S^2 \rangle_A$ = 0.00. We present the results in Table S11, observing (again) that the spin is located on the nitroso ligand ($\langle S^2 \rangle_3$ = 0.733) which contradicts again a Pd(I) situation. The off-diagonal terms (spin couplings) are quite small, indicating that the electron is mostly confined within the fragment.

Altogether, experimental evidence and quantum chemical simulations indicate that the system is best described as a Pd (II) complex featuring a ligand-centered radical delocalized over the nitroso metallacycle, rather than a true Pd(I) species.

Complex **2a** is not a unique compound. The same reaction (threefold excess of hydroxylamine) was also performed with differently substituted substrates. In the cases of 2-PhC_6H_4NHOH (**1e**) and 2-MeC_6H_4NHOH (**1f**), the product precipitated out of the reaction mixture, as observed also for **2a**, and an analogous structure can be proposed based on the detection of the molecular mass peaks of **2e** and **2f** in their ESI spectrum. When no substituent or fluoro or chloro substituents were present at the *para* position, only apparently incomplete reactions occurred, without any precipitate formation. However, when 2,6-$Me_2C_6H_3NHOH$ (**1b**) was employed, where both *ortho* positions were blocked and the coupling observed in **2a** could not occur, no reaction was observed (Scheme 1b). Full characterization is in progress for a series of metallacycles of type **2** together with an investigation of the mechanism by which they are formed.

Conclusions

In conclusion, we have prepared and characterized a complex that looked at first sight as a very rare example of a monomeric palladium(I) complex, but which turned out to be an equally rare case of a crystallographically characterized complex of a radical anionic nitrosoarene ligand. An extensive theoretical study has allowed us to describe in detail its electronic structure. The obtained complex is not a unique compound, and other complexes of the same class have also been obtained and preliminarily identified.

Experimental

Materials and methods

The solvents employed in this work were dried and degassed using standard procedures. Both acetonitrile and triethylamine were distilled from calcium hydride and stored under a dinitrogen atmosphere prior to use. Diethyl ether was distilled from sodium/benzophenone and stored under dinitrogen. 1,10-Phenanthroline (Phen), purchased as the hydrate, was dried by dissolution in CH_2Cl_2 followed by treatment with Na_2SO_4, filtration under nitrogen, and evaporation of the solvent under reduced pressure. The dried Phen was then stored under dinitrogen. Phenanthroline can be weighed in the air but must be stored under an inert atmosphere to avoid water uptake. Pd(Phen)$(OAc)_2$ was prepared as previously reported.[33] All glassware and magnetic stirring bars were dried in an oven at 120 °C for at least 2 h and allowed to cool under vacuum prior to use. All reactions were carried out under a dinitrogen atmosphere.

General method for preparation of *N*-aryl hydroxylamines

The employed hydroxylamines were synthesized following an adapted procedure reported in the literature.[8] In a 50 mL flask, nitroarene (2.0 mmol) and $NaBH_4$ (151 mg, 4.0 mmol) were dissolved in a mixture of H_2O/EtOH (8 mL/12 mL) and then 0.2 mL of 10 mM $Pd(OAc)_2$ solution (prepared by dissolving 9 mg of $Pd(OAc)_2$ in 4 mL CH_2Cl_2) was added. The mixture was stirred at room temperature until full consumption of the nitroarene as monitored by TLC (20–60 minutes). The reaction mixture was then directly extracted with CH_2Cl_2 or EtOAc. The combined organic layers were dried using anhydrous Na_2SO_4, filtered and concentrated, and then recrystallized with CH_2Cl_2/*n*-hexane to afford the corresponding hydroxylamine. Spectral data are in agreement with those reported in the literature.[8,34]

4-(Hydroxylamino)benzonitrile (1a)

1a was prepared according to general synthesis from 4-nitrobenzonitrile (296 mg, 2.0 mmol). The product was obtained as a white solid (212 mg, 79% yield). ^{1}H NMR (400 MHz, $CDCl_3$) δ 7.54 (d, J = 8.8 Hz, 2H, 2Ar–H), 7.01 (d, J = 8.8 Hz, 3H, 2Ar–H + NH), 5.44 (s, 1H, OH). ^{13}C NMR (101 MHz, $CDCl_3$) δ 153.74, 133.50, 119.14, 113.77, 104.31. Spectral data are in agreement with those reported in the literature.[8]

N-(2,6-Dimethylphenyl)hydroxylamine (1b)

1b was prepared according to general synthesis from 1,3-dimethyl-2-nitrobenzene (302 mg, 2.0 mmol). The product was obtained as a white solid (206 mg, 75% yield). ^{1}H NMR (400 MHz, DMSO) δ 7.08–6.95 (m, 3H, 3Ar–H), 6.86 (brs, 1H, NH), 5.12 (s, 1H, OH), 2.40 (s, 6H, $2CH_3$). ^{13}C NMR (101 MHz, $CDCl_3$) δ 144.33, 132.11, 128.95, 126.02, 18.00. Spectral data are in agreement with those reported in the literature.[34]

General procedure for the synthesis of Pd/*N*-arylhydroxylamine complexes

In an oven-dried Schlenk tube, Pd(Phen)$(OAc)_2$ (0.10 mmol) was dissolved in distilled acetonitrile (2.5 mL) and stirred until

complete dissolution (gentle warming was sometimes required to ensure full solubility). In a separate oven-dried Schlenk tube, the *N*-arylhydroxylamine derivative (0.30 mmol) was dissolved in acetonitrile (2.5 mL) and then added dropwise to the Pd(II) solution. An immediate colour change from yellow to green was observed upon addition of the *N*-arylhydroxylamine solution.

In the experiment where triethylamine was used to neutralize the acetic acid formed during the reaction, *p*-NCC_6H_4NHOH (0.10 mmol) was employed. Et_3N (0.10 mmol) was added to the reaction mixture immediately after the addition of the *N*-arylhydroxylamine derivative. In a separate trial, the order of addition was reversed, and the Pd(II) solution was added dropwise to the *N*-arylhydroxylamine solution; however, no difference in the outcome of the reaction was observed.

Although precipitation of the complex began approximately 2 h after the start of the reaction, the reaction mixture was allowed to stir for 48 h to ensure complete complex formation and to avoid the presence of residual unreacted Pd(II) in the final product. The resulting complex was collected by filtration and dried under reduced pressure.

2a: The isolated solid contains one cocrystallised molecule of water. 153.3 mg, 57.0% yield. Anal. calcd for $C_{26}H_{17}N_6O_2Pd$ (**2a**·H_2O): C, 56.59; H, 3.11; N, 15.23. Found: C, 56.49; H, 3.00; N, 14.95. Additional material was obtained by adding diethyl ether to the reaction solution after filtration, but it was not pure.

Crystallization of 2a

The complex was prepared according to the general procedure described above. Owing to its poor solubility in most common solvents, we investigated its recrystallization from acetonitrile, in which it shows slightly better solubility. In a narrow Schlenk tube, 15 mg of the complex was dissolved in acetonitrile (4 mL); gentle warming was required to ensure complete dissolution. After cooling to room temperature, the solution was further cooled to −30 °C. Once −30 °C was reached, diethyl ether (16 mL) was carefully layered along the wall of the Schlenk tube to avoid immediate mixing with the Pd–complex solution. The layered system was then allowed to slowly warm to room temperature and left undisturbed until complete diffusion of the diethyl ether had occurred. The solvents were subsequently removed carefully to afford green crystals of the complex, which were suitable for single-crystal X-ray diffraction analysis.

An initial attempt to isolate the crystals involved careful layering of diethyl ether directly onto the crude reaction mixture. Under these conditions, both green crystals of the desired complex and yellow crystals of $Pd(Phen)(OAc)_2$ were obtained.

Single crystal X-ray diffraction

A suitable 0.26 × 0.05 × 0.02 mm^3 crystal of **2a** was selected under a microscope, immersed in protective perfluoro–ether oil, and mounted on a goniometer head on a Rigaku XtaLAB Synergy, Dualflex diffractometer, equipped with an Oxford Cryosystem 800+ cryostat and a Hpyx-6000 hybrid pixel detector. X-ray diffraction was performed using microsource Cu-Kα radiation at T = 173 K. The structure was solved with the ShelXT[35] program using the intrinsic phasing solution method and by using Olex2[36] as the graphical interface. The model was refined with the version of olex2.refine 1.5[37] using Gauss–Newton minimisation. All non-hydrogen atoms were refined anisotropically. Hydrogen atom positions were calculated geometrically and refined using the riding model.

The structure contains large voids, likely occupied by the crystallization solvent, which is however not ordered and therefore invisible from the diffraction experiment. The asymmetric unit void has a volume of 107 Å^3 associated with *ca.* 23 electrons from the calculated Fourier difference map. This would correspond approximately to one molecule of CH_3CN in each asymmetric unit that contains a molecule of **2a**, giving therefore the final formula of $C_{26}H_{15}N_6OPd{\cdot}C_2H_3N$. For the final model refinement, the solvent mask option in Olex2 was applied, thus removing the contribution of the solvent from the structure factors. The presence of anions in the voids (that would imply a cationic complex) can be safely excluded because, if present, they would be more strongly bound to the complex. Moreover, the observed magnetism of **2a** clearly implies a neutral complex.

EPR spectroscopy

Powder EPR spectra of different samples of **2a** were measured on a Bruker E500 spectrometer using a SHQ cavity. The solution was bubbled with N_2 prior to measurement to reduce the broadening induced by dissolved O_2 and increase resolution. Low temperature was achieved by using a ^{4}He continuous flow ESR900 cryostat (Oxford Instrument). The EPR spectra of microcrystalline powder samples and frozen solution were simulated by using the *pepper* function of EasySpin,[21] while for fluid solution simulation *garlic* was used. The simulation of the immobilized samples assumed an anisotropic S = 1/2 spin Hamiltonian either including (frozen solution) or not (microcrystalline powder) the hyperfine coupling to nitrogen: $\hat{H}_{\mathrm{aniso}} = \beta\hat{\boldsymbol{S}}\cdot\boldsymbol{g}\cdot\vec{\boldsymbol{B}} + \hat{\boldsymbol{S}}\cdot\boldsymbol{A}\cdot\hat{\boldsymbol{I}}$, where β is the Bohr magneton. Solution spectra were simulated assuming an isotropic spin Hamiltonian including hyperfine coupling to one ^{14}N, one ^{1}H, and ^{105}Pd (the latter for a fraction of 22%, according to its natural abundance):

$$\hat{H}_{\mathrm{iso}} = \beta g_{\mathrm{iso}}\hat{\boldsymbol{S}}\cdot\vec{\boldsymbol{B}} + {}^{\mathrm{N}}A_{\mathrm{iso}}\hat{\boldsymbol{S}}\cdot{}^{\mathrm{N}}\hat{\boldsymbol{I}} + {}^{H}A_{\mathrm{iso}}\hat{\boldsymbol{S}}\cdot{}^{H}\hat{\boldsymbol{I}} + {}^{\mathrm{Pd}}A_{\mathrm{iso}}\hat{\boldsymbol{S}}\cdot{}^{\mathrm{Pd}}\hat{\boldsymbol{I}}$$

Author contributions

D. R. Ramadan, M. A. Fouad, F. Ferretti, A. Brotons Rufes, P. Macchi, L. Sorace, and M. Gimferrer: investigation, writing – original draft, and writing – review & editing. C. Costabile and F. Ragaini: conceptualization, funding acquisition, project administration, supervision, writing – original draft, and writing – review & editing.

Conflicts of interest

There are no conflicts to declare.

Data availability

The supporting data have been provided as a part of the supplementary information (SI). Supplementary information: Tables S1–S12, NMR and UV spectra, check-CIF file, magnetic data and further experimental details. Ref. 38–48 are cited in the SI. See DOI: https://doi.org/10.1039/d6dt01038e.

CCDC 2521055 (**2a**) contains the supplementary crystallographic data for this paper.[49]

Acknowledgements

The project was funded by the European Union – Next Generation EU, Mission 4 Component 1 CUP_ G53D23003450006 and CUP_ D53D23010540006, and the University of Salerno (FARB). We acknowledge ISCRA for awarding these project accesses (HP10C2EN0Q and HP10C74PPF) to the LEONARDO supercomputer, owned by the EuroHPC Joint Undertaking, hosted by CINECA (Italy). The authors gratefully acknowledge the Computing Cluster Phoenix HPC at the Department of Chemistry and Biology "A. Zambelli", University of Salerno, Italy. L. S. acknowledges the financial support provided by the MUR – Dipartimenti di Eccellenza 2023–2027 (DICUS 2.0) (ref no. B97G22000740001) to the Department of Chemistry "Ugo Schiff" of the University of Florence. M. G. acknowledges funding by the German Research Foundation (DFG) *via* project 389479699/GRK2455. The single crystal diffraction experiment was carried out at the Next GAME Laboratory of the Politecnico di Milano, co-funded by Regione Lombardia. We thank Stefano Miele for performing some reactions.

References

1 F. Ferretti, D. R. Ramadan and F. Ragaini, *ChemCatChem*, 2019, **11**, 4450–4488.
2 F. Ragaini, *Dalton Trans.*, 2009, 6251–6266.
3 A. A. Tsygankov, M. Makarova and D. Chusov, *Mendeleev Commun.*, 2018, **28**, 113–122.
4 B. R. Barnett, L. A. Labios, C. E. Moore, J. England, A. L. Rheingold, K. Wieghardt and J. S. Figueroa, *Inorg. Chem.*, 2015, **54**, 7110–7121.
5 N. C. Tomson, L. A. Labios, T. Weyhermüller, J. S. Figueroa and K. Wieghardt, *Inorg. Chem.*, 2011, **50**, 5763–5776.
6 E. Gallo, F. Ragaini, S. Cenini and F. Demartin, *J. Organomet. Chem.*, 1999, **586**, 190–195.
7 F. Ferretti, M. Rimoldi, F. Ragaini and P. Macchi, *Inorg. Chim. Acta*, 2018, **470**, 284–289.
8 Z. Yan, X. Xie, Q. Song, F. Ma, X. Sui, Z. Huo and M. Ma, *Green Chem.*, 2020, **22**, 1301–1307.
9 M. Cameron, B. G. Gowenlock and G. Vasapollo, *Chem. Soc. Rev.*, 1990, **19**, 355–379.
10 S. Banerjee, S. Chakrabarti, B. S. Bouley, A. J. Wahlmeier and L. M. Mirica, *Coord. Chem. Rev.*, 2025, **535**, 216605.
11 T. Bruckhoff, J. Ballmann and L. H. Gade, *Angew. Chem., Int. Ed.*, 2024, **63**, e202320064.
12 G. N. Tran, B. S. Bouley and L. M. Mirica, *J. Am. Chem. Soc.*, 2022, **144**, 20008–20015.
13 S. T. Orlova, T. A. Stromnova, D. N. Kazyul'kin, L. I. Boganova, D. I. Kochubey and B. N. Novgorodov, *Russ. Chem. Bull.*, 2004, **53**, 819–824.
14 I. L. Eremenko, S. E. Nefedov, A. A. Sidorov, M. O. Ponina, P. V. Danilov, T. A. Stromnova, I. P. Stolarov, S. B. Katser, S. T. Orlova, M. N. Vargaftik, I. I. Moiseev and Y. A. Ustynyuk, *J. Organomet. Chem.*, 1998, **551**, 171–194.
15 S. Wirth, A. U. Wallek, A. Zernickel, F. Feil, M. Sztiller-Sikorska, K. Lesiak-Mieczkowska, C. Bräuchle, I.-P. Lorenz and M. Czyz, *J. Inorg. Biochem.*, 2010, **104**, 774–789.
16 L. A. Labios, M. D. Millard, A. L. Rheingold and J. S. Figueroa, *J. Am. Chem. Soc.*, 2009, **131**, 11318–11319.
17 Y. Gao, S. Yang, W. Xiao, J. Nie and X.-Q. Hu, *Chem. Commun.*, 2020, **56**, 13719–13730.
18 S. Wiese, P. Kapoor, K. D. Williams and T. H. Warren, *J. Am. Chem. Soc.*, 2009, **131**, 18105–18111.
19 N. C. Tomson, K. D. Williams, X. Dai, S. Sproules, S. DeBeer, T. H. Warren and K. Wieghardt, *Chem. Sci.*, 2015, **6**, 2474–2487.
20 S. Kundu, S. C. E. Stieber, M. G. Ferrier, S. A. Kozimor, J. A. Bertke and T. H. Warren, *Angew. Chem., Int. Ed.*, 2016, **55**, 10321–10325.
21 S. Stoll and A. Schweiger, *J. Magn. Reson.*, 2006, **178**, 42–55.
22 M. G. Swanwick and W. A. Waters, *J. Chem. Soc. D*, 1970, 930–931.
23 G. Gronchi and P. Tordo, *Res. Chem. Intermed.*, 1993, **19**, 733–753.
24 D. Wang, M. Tamizmani, X. Leng and L. Deng, *Chin. J. Chem.*, 2020, **38**, 158–162.
25 S. B. H. Karnbrock, J. F. Köster, I. Becker, C. Golz, F. Meyer, M. Gimferrer and M. Alcarazo, *Chem. Sci.*, 2025, **16**, 14178–14185.
26 M. Gimferrer, P. Salvador and A. Poater, *Organometallics*, 2019, **38**, 4585–4592.
27 G. Comas-Vilà and P. Salvador, *Inorg. Chem.*, 2025, **64**, 15437–15447.
28 P. Salvador, E. Ramos-Cordoba, M. Montilla, L. Pujal and M. Gimferrer, *J. Chem. Phys.*, 2024, **160**, 172502.
29 P. Salvador and E. Ramos-Cordoba, *J. Chem. Phys.*, 2013, **139**, 071103.
30 I. Mayer and P. Salvador, *Chem. Phys. Lett.*, 2004, **383**, 368–375.
31 M. Gimferrer, J. Van der Mynsbrugge, A. T. Bell, P. Salvador and M. Head-Gordon, *Inorg. Chem.*, 2020, **59**, 15410–15420.
32 K. Takatsuka, T. Fueno and K. Yamaguchi, *Theor. Chim. Acta*, 1978, **48**, 175–183.
33 F. Ragaini, M. Gasperini, S. Cenini, L. Arnera, A. Caselli, P. Macchi and N. Casati, *Chem. – Eur. J.*, 2009, **15**, 8064–8077.

34 F. Wang, O. Planas and J. Cornella, *J. Am. Chem. Soc.*, 2019, **141**, 4235–4240.
35 G. M. Sheldrick, *Acta Crystallogr., Sect. A: Found. Adv.*, 2015, **71**, 3–8.
36 O. V. Dolomanov, L. J. Bourhis, R. J. Gildea, J. A. K. Howard and H. Puschmann, *J. Appl. Crystallogr.*, 2009, **42**, 339–341.
37 L. J. Bourhis, O. V. Dolomanov, R. J. Gildea, J. A. K. Howard and H. Puschmann, *Acta Crystallogr., Sect. A: Found. Adv.*, 2015, **71**, 59–75.
38 J. A. Weil and J. R. Bolton, *Electron Paramagnetic Resonance: Elementary Theory and Practical Applications*, John Wiley & Sons, Inc., Hoboken, New Jersey, 2007.
39 J. R. Morton and K. F. Preston, *J. Magn. Reson.*, 1978, **30**, 577–582.
40 M. J. Frisch, G. W. Trucks, H. B. Schlegel, G. E. Scuseria, M. A. Robb, J. R. Cheeseman, G. Scalmani, V. Barone, G. A. Petersson, H. Nakatsuji, X. Li, M. Caricato, A. V. Marenich, J. Bloino, B. G. Janesko, R. Gomperts, B. Mennucci, H. P. Hratchian, J. V. Ortiz, A. F. Izmaylov, J. L. Sonnenberg, D. Williams-Young, F. Ding, F. Lipparini, F. Egidi, J. Goings, B. Peng, A. Petrone, T. Henderson, D. Ranasinghe, V. G. Zakrzewski, J. Gao, N. Rega, G. Zheng, W. Liang, M. Hada, M. Ehara, K. Toyota, R. Fukuda, J. Hasegawa, M. Ishida, T. Nakajima, Y. Honda, O. Kitao, H. Nakai, T. Vreven, K. Throssell, J. A. Montgomery Jr., J. E. Peralta, F. Ogliaro, M. J. Bearpark, J. J. Heyd, E. N. Brothers, K. N. Kudin, V. N. Staroverov, T. A. Keith, R. Kobayashi, J. Normand, K. Raghavachari, A. P. Rendell, J. C. Burant, S. S. Iyengar, J. Tomasi, M. Cossi, J. M. Millam, M. Klene, C. Adamo, R. Cammi, J. W. Ochterski, R. L. Martin, K. Morokuma, O. Farkas, J. B. Foresman and D. J. Fox, *Gaussian 16 Rev. C.01*, Wallingford, CT, 2016.
41 A. D. Becke, *Phys. Rev. A*, 1988, **38**, 3098–3100.
42 J. P. Perdew, *Phys. Rev. B:Condens. Matter Mater. Phys.*, 1986, **33**, 8822–8824.
43 J. P. Perdew, *Phys. Rev. B:Condens. Matter Mater. Phys.*, 1986, **34**, 7406.
44 F. Weigend and R. Ahlrichs, *Phys. Chem. Chem. Phys.*, 2005, **7**, 3297–3305.
45 F. Weigend, *Phys. Chem. Chem. Phys.*, 2006, **8**, 1057–1065.
46 Y. Zhao and D. G. Truhlar, *Theor. Chem. Acc.*, 2008, **120**, 215–241.
47 S. Grimme, J. Antony, S. Ehrlich and H. Krieg, *J. Chem. Phys.*, 2010, **132**, 154104.
48 G. Scalmani and M. J. Frisch, *J. Chem. Phys.*, 2010, **132**, 114110.
49 CCDC 2521055: Experimental Crystal Structure Determination, 2026, DOI: 10.5517/ccdc.csd.cc2qmcc3.